UCLA
Department of Statistics Papers

Title

Classification of Spatially Unaligned fMRI Scans

Permalink

https://escholarship.org/uc/item/9zx0g2n6

Authors

Ariana Anderson
Ivo D. Dinov
Jonathan E. Sherin
et al.

Publication Date

2011-10-25

Classification of spatially unaligned fMRI scans
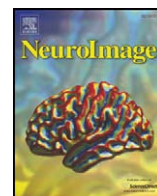
Ariana Anderson [a,b], Ivo D. Dinov [a,e], Jonathan E. Sherin [c,f], Javier Quintana [c,f],
A.L. Yuille [g,h], Mark S. Cohen [b,c,d,*]

[a] Department of Statistics, UCLA, Los Angeles, CA 90095, USA
[b] Center for Cognitive Neuroscience, UCLA, Los Angeles, CA 90095, USA
[c] Department of Psychiatry and Behavioral Sciences, UCLA, Los Angeles, CA 90095, USA
[d] UCLA School of Medicine, Los Angeles, CA 90095, USA
[e] Center for Computational Biology, UCLA, Los Angeles, CA 90095, USA
[f] Greater Los Angeles VA Healthcare System, Los Angeles, CA 90095, USA
[g] Department of Computer Science, UCLA, Los Angeles, CA 90095, USA
[h] Department of Psychology, UCLA, Los Angeles, CA 90095, USA

ABSTRACT

The analysis of fMRI data is challenging because they consist generally of a relatively modest signal contained in a high-dimensional space: a single scan can contain over 15 million voxel recordings over space and time. We present a method for classification and discrimination among fMRI that is based on modeling the scans as distance matrices, where each matrix measures the divergence of spatial network signals that fluctuate over time. We used single-subject independent components analysis (ICA), decomposing an fMRI scan into a set of statistically independent spatial networks, to extract spatial networks and time courses from each subject that have unique relationship with the other components within that subject. Mathematical properties of these relationships reveal information about the infrastructure of the brain by measuring the interaction between and strength of the components. Our technique is unique, in that it does not require spatial alignment of the scans across subjects. Instead, the classifications are made solely on the temporal activity taken by the subject's unique ICs. Multiple scans are not required and multivariate classification is implementable, and the algorithm is effectively blind to the subject-uniform underlying task paradigm. Classification accuracy of up to 90% was realized on a resting-scanned schizophrenia/normal dataset and a tasked multivariate Alzheimer's/old/young dataset. We propose that the ICs represent a plausible set of imaging basis functions consistent with network-driven theories of neural activity in which the observed signal is an aggregate of independent spatial networks having possibly dependent temporal activity.

© 2009 Elsevier Inc. All rights reserved.

Introduction

Existing neuroimaging classification methods for functional magnetic resonance imaging (fMRI) data have shown much promise in discriminating among cerebral scans, but are limited in the types of data they can handle, and in the numbers of outcomes they can predict (Ford et al., 2003; Zhang and Samaras, 2005). In general, fMRI discrimination methods require preprocessing steps such as spatial alignment of the scans and are only infrequently suitable for multivariate classification problems (Calhoun et al., 2007) because of their utilization of bivariate classifiers. Spatial alignment algorithms often are constructed assuming a subject has a normal brain, and therefore may be less accurate when warping scans of patients with physical anomalies. Existing classification methods typically require

knowledge of the task paradigm thereby limiting their application to subjects who are able and willing to perform such tasks. Here we introduce a procedure called *spectral classification* that is capable of multivariate discrimination among single-session fMRI scans taken during both a tasked and "mind-wandering" (task-free) state. The methods classify based on the *temporal* structure of the data rather than the spatial structure, thereby bypassing the need for spatial alignment of the scans. We call this method spectral classification because of its usage of spectral graph-theory measurements for discrimination. We demonstrate here a non-spatial method of classification having cross-validation accuracy rates as high as 90% for bivariate classification. Mathematically we introduce a method for comparing and classifying objects represented by distance matrices. In this paper an entire matrix describes an fMRI scan where the entries contain the "distances" between the activity of two components' timeseries; however these methods are generally applicable to any problem in which the elements are described as matrices rather than isolated points and discrimination is desired among these objects.

* Corresponding author. UCLA Center for Cognitive Neuroscience, Suite C8-881, 740 Westwood Plaza, Los Angeles, CA 90095, USA. Office: +1 310 986 3307; Lab: +1 310 825 9142.
E-mail address: mscohen@ucla.edu (M.S. Cohen).

Temporally recorded neuroimaging data pose a unique challenge to classification because of the high-dimensional structure of the data sets. One scan can contain more than 120,000 recordings that often are highly correlated both in only four effective dimensions consisting of space and time. Because of this, practical classification procedures require an initial dimension-reduction stage where discriminating signal is extracted from the noisy data. In spatial-based discrimination methods, localized summaries of the temporal signal are used to compress the temporal dimension into a single point at every spatial location. The spatial regions containing discriminating summary statistics are extracted and used to create a classification machine. (Zhang and Samaras, 2005; Ford et al., 2003).

The summary statistics used for describing temporal activity include mean signal intensities or p-values measuring association with a known task-paradigm. These regional summary statistics are compared across subjects when training the classifier, requiring the scans be spatially aligned to a common atlas space. The most often used alignment algorithms (Woods et al., 1998) are 12-parameter affine transformations that warp a subject's brain to a common atlas space. Alignment precision is limited with normal patients by the low geometric flexibility of the algorithms, and is potentially more difficult to achieve with subjects having structural inconsistencies associated with mental disorders. For example, it is known that people with schizophrenia have significantly larger ventricles (Shenton et al., 2001) and that Alzheimer's sufferers show brain atrophy (Ridha et al., 2006); standard structural alignment tools cannot take into account the unique differences existing in these patients. Thus, spatially based discrimination methods may fail in classifications across individuals due simply to poor spatial alignment.

A known task function is often correlated regionally with timeseries to identify regions closely associated with a task. Improved alignment methods notwithstanding, localized low-order summary statistics of the regional BOLD signal may not capture higher-order discriminating information contained in the temporal domain. If functional anatomy is similar among patient groups, then the temporal information of the scans offer a new dimension with potentially discriminative information. If the group differences exist not in the spatially localized signal summary but in the native temporal activity taken by the brain, classification methods relying on summary statistics could fail to distinguish between groups. A method that instead reduced the often-redundant spatial dimension while keeping intact the temporal structure would capitalize on signal differences existing in the temporal domain rather than spatial. The method proposed here is agnostic to the task function and yields similar accuracy results discriminating among identically tasked scans and untasked scans in two datasets tested here.

Because of the limitations of spatial discrimination methods, there is a need for a classification method that is both insensitive to spatial alignment and independent of low order statistical summaries. Using unaligned scans our method classifies on temporal activity patterns between independent components within a subject. The blind source separation method of independent components analysis (ICA) is capable of decomposing a sequence of three-dimensional images into sources consisting of statistically independent spatial maps acting over time according to possibly dependent activity patterns. When applied to fMRI data, ICA decomposes a four-dimensional single fMRI scan into a set of statistically independent spatial components (Hyvärinen and Oja, 2000). These spatially independent components have corresponding time courses that show statistical dependence with the time courses of other components. The strength of the relationship between components is indicated by coupling, or correlated intensities over time.

It is not known which if any of the spatial components identified by ICA represent functional neural networks, however it has previously been shown that ICA-methods yield identifiable stable neurological patterns. Damoiseaux et al. (2006) were able to identify 10 consistent resting state networks common across their population that appear to correspond to identifiable phenomena such as motor function, visual processing, executive functioning, auditory processing, memory, and even the default-mode network, however the identification of these components is not required with our approach to classification yet remains a hidden layer that might be useful for neuroscientific interpretation. The general goal of our work is to develop a classification method that is independent of any trained user interaction making the tool more practically applicable and less sensitive to experimenter bias. One consequence of this, as implemented here, is that the classification itself may be based on signals that are not directly interpretable as neural in nature. For example, it is possible that group specific artifacts, such as head motion, might be contributing to the classifier. For the moment, we note that even in the face of this potential limitation, the classifier appears quite robust. In the future, we intend to use automated means to detect and reject identifiable artifacts (such as motion). Because the time courses alone are used for discrimination our method does not require us to associate the spatial components with a known biological process to classify a scan; rather, we are concerned with the temporal structure that these components take, how similar they are with other components in that subject, and how this dependency varies across subjects and groups.

In the classification method described here, inter-subject component comparisons do not require multiple scans or knowledge of the underlying task paradigm. We describe here the application of our methods using two separate datasets. The first consists of blocked-task designed scans from normal old, normal young, and Alzheimer's patients, while the second dataset consists of resting-state scans of Schizophrenia subjects and normal controls. We estimated the classification testing accuracy using cross-validation (C.V.) and the out-of-bag error from the random forests (R.F.) (Breiman, 2001) classifier, where the accuracy is an estimate of how well the classifier would do if given a new scan from a previously unseen subject.

Random forests is a decision-tree machine learning method that creates many classification trees by resampling from both the observations and classifiers at each node and subsequently making decision rules to minimize the misclassification rate of the sampled data within each tree. Many decision trees are constructed and combined to create a "forest" that decides an observation's class by voting over the decisions made by each tree. The tree is then tested on observations that weren't selected in the initial sampling, to give the "out-of-bag" error which is usually an unbiased estimate of the testing error.

Materials and methods

Overview

The first step in spectral classification is to perform ICA individually on the scans to reduce the dimensions of the data and extract the time courses of the components. We then create distance matrices that capture the relationship between the temporal signals within a subject, and extract features from these similarity matrices using the principal (largest) eigenvalues. Finally, we train a random forests classifier on the extracted features and evaluate the out-of-bag and cross-validation errors as measures.

The implementation of the spectral classification procedure can be summarized as follows:

- Step 1: Decompose a scan into spatial networks and timecourses using independent components analysis (ICA).
- Step 2: Create a distance matrix describing temporal correlations among spatial components within a subject.

- Step 3: "Unwrap" the distance matrix by calculating the geodesic distance among components and extract principal eigenvalues from distance matrix to create feature vector.
- Step 4: Train a (multivariate) random forests classifier using eigenvalues as features, and evaluate it by using cross-validation.

Data characteristics

All subjects, both schizophrenia patients and healthy controls, gave written informed consent and were recruited and studied under a protocol approved by the UCLA and the Greater Los Angeles VA Health Care System Institutional Review Boards. The schizophrenia/normal dataset consists of 14 clinically stable schizophrenia outpatients (diagnosed according to DSM-IV-R criteria using a structured clinical interview) and 6 healthy controls, matched to the affected individuals for age, gender, race, handedness and parental education level. Subjects were scanned at rest on a Siemens Allegra 3T scanner (Erlangen, Germany) in supine position, wearing acoustic noise protectors. To facilitate later coordinate alignments, we collected a high-resolution three-dimensional MPRAGE data set. (Scan parameters: TR/TE/TI/Matrix size/Flip Angle/FOV/Thickness = 2300/2.9/1100/160×192×192/20/256×256/1 mm). We then collected a set of T2-weighted EPI images (TR/TE/Matrix size/Flip Angle/FOV/Thickness = 5000/33/128×128×30/90/200×200/4.0 mm) with bandwidth matched to the later BOLD studies, covering 30 horizontal slices in the same plane of section used for activation studies. These data are inherently in register with the subsequently collected functional series as they share the same metric distortions. For the latter, multi-slice echo-planar imaging (EPI) was used to measure blood oxygenation level dependent (BOLD)-based signals (TR/TE/Matrix size/Flip Angle/ FOV/Thickness = 2500/45/64×64×30/90/200×200/4.0 mm) The fMRI procedure detects signal changes that indicate neuronal signaling indirectly through changes in signal intensity that reflect relative blood oxygenation and thus metabolic demands. We preprocessed the scans using motion correction (MCFLIRT in FSL) and then performed skull-stripping using FSL's BETALL (Smith et al., 2004).

The Alzheimer's young/old dataset was obtained from the fMRI Data Repository Center, collected originally by Randy Buckner (Buckner et al., 2000). A history of neurological or visual illness served as exclusion criteria for all potential subjects. Furthermore, older adults were excluded if they had neurologic, psychiatric or mental illness that could cause dementia. A total of 41 participants (14 young adults, 14 nondemented older adults, and 13 demented older adults) were included in the dataset. The task paradigm used an event-related design consisting of presentation of a 1.5-s visual stimulus. Subjects pressed a key with their right index fingers upon stimulus onset. The visual stimulus was an 8-Hz counterphase flickering (black to white) checkerboard subtending approximately 12 of visual angle (six in each visual field). Stimulus onset was triggered at the beginning of the image acquisition via the PsyScope button box.

The methods presented in this paper were performed using tools in FSL (Smith et al., 2004) and routines coded in R (R Development Core Team, 2008).

Constructing an automatic classifier required us to reduce the dimensionality of the data, construct activity manifolds on which to calculate the geodesic distances (Tenenbaum et al., 2000), create feature vectors using properties of these manifolds, and to perform classification of the subjects.

Dimension reduction

As fMRI data is very high dimensional it is necessary to first reduce the data in a manner that preserves its temporal structure. When ICA is performed on an fMRI scan, the data is broken down into a set of spatial activation maps and their associated time courses.

A scan of time length T and spatial dimension S and can be expressed as a linear combination of $N \leq T$ components and the corresponding timecourses:

$$X_{ts} = \sum_{\mu=1}^{N} M_{t\mu} C_{\mu s} \tag{1}$$

Where X_{ts} represents the raw scan intensity at timepoint $t \leq T$ and spatial location $s \leq S$, $M_{t\mu}$ is the amplitude of component μ at time t, and $C_{\mu s}$ is the spatial magnitude for component μ at spatial location s.

In the ICA decomposition, the spatial components are assumed to be statistically independent, however, there is no assumption of independence for their time courses. ICA is run on each subject, extracting all relevant components that are found within that subject. The Laplacian approximation to the model order is used to derive the number of components existing in each subjects, as has been found effective in estimating the underlying number of signal sources (Minka, 2000). The consequences of using other methods to determine the number of components are discussed in Sensitivity to component number approximation method.

The net result is that the dimensionality is reduced from an initially four-dimensional dataset into a selection of time series and a small number of spatial maps representing the spatial signatures of the independent components within a subject. We use the time series of the components for classification as they are not dependent on proper spatial alignment over the population. In addition, the time series represent a more compact description of the data than the spatial maps because of the smaller dimensionality of a one-effective dimension timeseries compared to a three-effective dimension spatial map. This in turn allows for more flexibility in the discrimination methods available because of computational efficiency.

Manifold construction

Each independent component can be considered a node on an unknown graph or manifold unique to each subject, and we can model the connection between two nodes by measuring the similarity between two components' timeseries. The metric of similarity presented here is based on the measure of cross-correlation, but the classification methods were tested successfully also with frequency domain signal strength, fractal dimension, and standard statistical correlation.

Graphically we want to measure the randomness taken by the bivariate path of two components. Let M_α and M_β be the timecourses from two different independent components within a subject. The bivariate plot of the first and second timecourse within two random subjects is shown in Fig. 1, where the two timecourses are selected as being those that explain the most variance out of all extracted timecourses, and are unique within each subject. We wish to see if the patterns observed in the interactions of components are consistent and strong enough to discriminate among patient groups.

To quantify the relatedness between pairs of temporal components we compute a distance metric based on the cross-correlation function, which is a linear measure of the similarity between two time series and may be computed for a wide range of lags. Time series based measures have been used to explore directed influences between neuronal populations in fMRI data (Roebroeck et al., 2005) using Granger causality and have found increased correlation among independent components in schizophrenia patients compared to normal controls (Jafri et al., 2007) using the cross-correlation. We used the maximal absolute correlation between two time series over a range of lags as an indicator of the amount of information shared
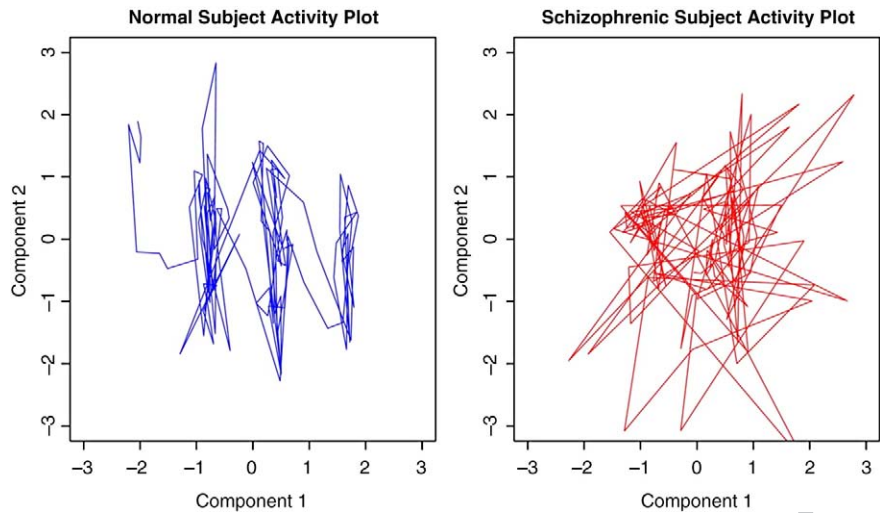
Fig. 1. Phase space for primary components.

331 between them and how similarly they act over time.

$$\mathrm{CCF}\left(M_\alpha, M_\beta, l\right) = \frac{E\left[\left(m_{\alpha,t+l} - \overline{M_\alpha}\right)\left(m_{\beta,t} - \overline{M_\beta}\right)\right]}{\sqrt{E\left[\left(m_{\alpha,t} - \overline{M_\alpha}\right)^2\right]E\left[\left(m_{\beta,t} - \overline{M_\beta}\right)^2\right]}} \quad (2)$$

333 where $m_{\alpha,t+l}$ is time-shifted version, $m_{\alpha,t}$, l is the time lag separating
334 the two timeseries M_α and M_β, and M_α is the mean of the entire
335 timeseries $M_\alpha = (m_{\alpha,1}, m_{\alpha,2}, \ldots, m_{\alpha,T})$. The timeseries are calculated
336 at lags ranging from 0 to 20% of the timeseries length, as higher lags
337 results in fewer time points to calculate the correlation and a more
338 noisy estimate. The distance function is a transformation of the
339 maximal absolute cross-correlation between two timeseries.

$$d\left(M_\alpha, M_\beta\right) = \frac{1}{\max_{\text{lags}}\left[\left|\mathrm{CCF}\left(M_\alpha, M_\beta\right)\right|\right]} - 1 \quad (3)$$

340 To test the dependency of our method on a particular metric, we
342 compared the results of our chosen metric with three other distance
343 metrics derived from the raw correlation, fractal dimension, and a
344 measure of Fourier signal strength. Similar accuracy results were
345 obtained which are discussed further in Table 3.4.
346   Within a subject i calculating the distance between all N_i temporal
347 components yields a distance matrix $\Phi_{N_i \times N_i}$. The dimensionality of
348 each subject's matrix corresponds to the number of independent
349 components initially extracted as shown in Fig. 2 and may therefore
350 differ. The darker intensity in Fig. 2 indicates a smaller distance, while
351 a lighter color shows a greater distance. The distances range in value

from (0, 9) and the colors are normalized within each matrix so that 352
darkest lightest color corresponds to the greatest intensity. The rows 353
and columns in the distance matrices have no direct correspondence 354
across subjects. The temporal components are extracted individually 355
within each subject using ICA, leading to a unique structure in the 356
temporal associations within that subject's distance matrix, $\Phi_{N_i \times N_i}$. 357

Feature selection 358

   Each matrix $\Phi_{N_i \times N_i}$ represents the connectivity over time of 359
independent components M_α embedded on some unknown manifold 360
that is unique to each subject. Distances between points $d(M_\alpha, M_\beta)$ 361
quantify the temporal similarity between two components repre- 362
sented by timeseries M_α and M_β. It is unreasonable to assume that the 363
graphical structure represented by a matrix for subject i, $\Phi_{N_i \times N_i}$, lies 364
on a linear space, as only a very small subset of all the spaces on which 365
a manifold could lie will be linear. To account for this, an intermediary 366
step will be performed prior to feature extraction that will warp the 367
graphical structures represented by the matrices to account for the 368
potential non-linearity of the manifolds. 369
   The matrices are warped for each subject using the same principles 370
underlying the manifold embedding technique of ISOMAP (Tenen- 371
baum et al., 2000). Within each subject, the original matrix is 372
transformed by recalculating the distances among components using 373
a non-linear metric, the *geodesic distance* (Tenenbaum et al., 2000). 374
The geodesic distance measures distances between non-neighboring 375
points as the shortest path connecting points *through* their neighbors 376
as in Fig. 3, where the distance between A and C is calculated as the 377
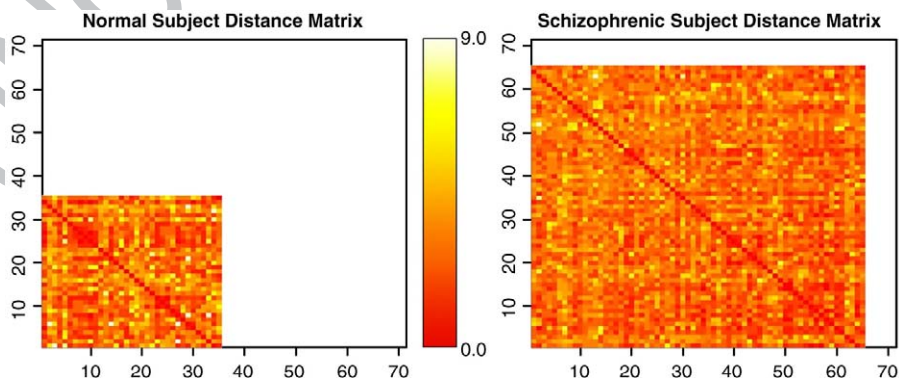manifold path distance from A to B to C instead of directly from A to C. 378

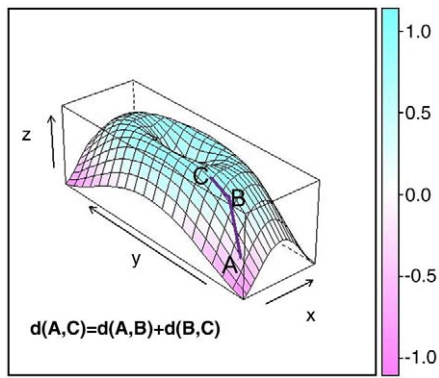**Fig. 2.** Subject matrices showing unequal number of component.

Fig. 3. Geodesic distance calculation.

$$d(A,C)=d(A,B)+d(B,C)$$

Points are considered connected if they fall within a set of *k*-nearest neighbors, where *k* is chosen to minimize the Bayesian Information Criterion (BIC) (Hogg et al., 2000) of the goodness of fit within the subject. Further discussion on the choice of neighborhood size and embedding dimension in presented in Sensitivity to parameter choice. Using the geodesic distance, each matrix $\Phi_{N_i \times N_i}$ is warped separately by recalculating the distances among points (components) prior to extracting features to create a new matrix $\Phi^*_{N_i \times N_i}$.

We illustrate the graphical structures these matrices $\Phi^*_{N_i \times N_i}$ represent by embedding them individually in a two-dimensional space using ISOMAP, shown in Fig. 4. To perform the embedding the distance matrix is projected onto the eigenvectors corresponding to the two principal eigenvalues of the decomposition of the geodesic distance matrix (Tenenbaum et al., 2000; Kruskal and March, 1964). Every vertex represents an independent component, while the edge length between vertices corresponds to the geodesic distance between two components. The complete relationship of *spectral classification* to other methods such as ISOMAP is discussed in Relationship to existing methods.

The manifold defined by $\Phi^*_{N_i \times N_i}$ can be described by the eigenvalues λ of the distance matrix that measure the *variance explained* along the different dimensions. $\Phi^*_{N_i \times N_i} = Q \wedge Q^{-1}$ where Q is the matrix of eigenvectors and $\wedge$ is the matrix of eigenvalues. The largest $n_i \leq N_i$ eigenvalues for subject *i* are used to create a feature vector $\overleftarrow{\lambda}_i = (\lambda_{1_i}, \lambda_{2_i}, \dots, \lambda_{n_i})$. Extracting eigenvalues from each graph bypasses the issue of the structures all lying on a unique self-defined manifold, because we are using the properties of the subjects' manifolds to classify instead of the points (components) comprising it. For classification purposes we enforce that $n_i = c \; \forall i$ where *c* is some constant chosen as in Sensitivity to parameter choice, because it is necessary to use the same number of features for classification per subject. The principal eigenvalues of the geodesic distance matrix give the strength along the primary dimension and reveal the "skew" in the connective structure of the components. The geodesic distance matrix is analogous to the weighted adjacency matrix of the graph; hence, the spectral decomposition of this matrix lends itself to the procedure name of *spectral classification*.

Subject classification

Once feature vectors $\overleftarrow{\lambda}$ have been extracted for all subjects a classifier is trained using Random Forests (Breiman, 2001). Random Forests is well-suited for multivariate classification problems as it decides outcomes by voting, and is less likely to overfit in practice than other methods because of its usage of resampling. The algorithm operates by repeatedly sampling from the data and predictors to construct decision trees. A group of classification trees become a *forest*, which classifies an observation by having the trees that had not previously seen that observation vote for an outcome. The predicted class of an observation is taken to be the category with the maximal votes by all the trees. The cross-validation error of the classification forest is taken to be the *out-of-bag* error, and the average error is taken to be the best estimate of the accuracy of this predictor on a completely new scan. However, because the parameters are selected with respect to the out-of-bag error, the testing error is biased. Because of this, we performed cross-validation outside of the parameter selection process to obtain an unbiased testing error estimate.

Results and discussion

The spectral classification procedure was run on both the schizophrenia/normal and the Alzheimer's/old/young dataset to obtain bivariate and multivariate classification results. The Alzheimer's/old/young dataset was also grouped into pairs to further test bivariate classification. There were two parameters involved in fitting the manifold: the neighborhood size, *k*, and n_i, the number of dimensions in which to embed. We present the results using two different parameter selection methods. For more details on these selection methods see Method 1: Single parameter optimization.

Method 1: Optimized single parameter selection

We will describe here a method of selecting model parameters (n, k_i) such that k_i is selected within a subject by optimizing a model fit, and *n* is optimized with respect to minimizing the classification error over all subjects. The embedding dimension *n* is a global parameter
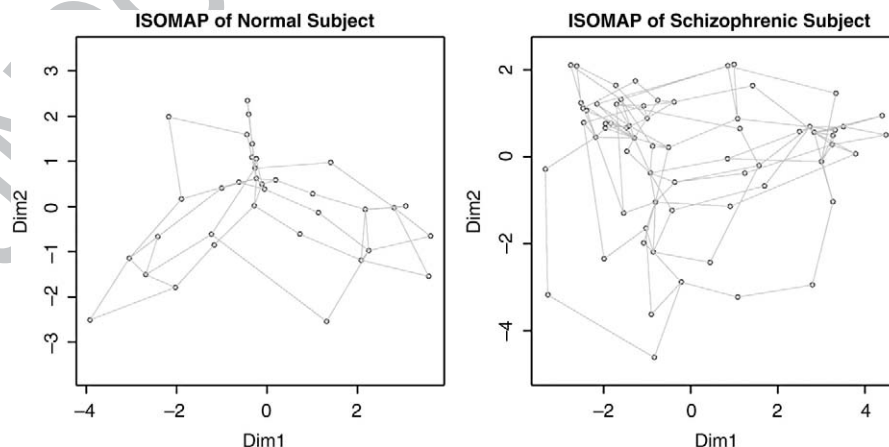

Fig. 4. Embedding of matrices.

held constant for all subjects, while k_i is allowed to vary within subject.

For a given n we will select the fitting parameter k_i within a subject by minimizing the Bayesian Information Criterion (BIC) for the goodness of fit. The goodness of fit measure, L_i, is the sum of the eigenvalues used in the partial fitting normalized by the total absolute value of all the eigenvalues.

$$L_i = \frac{\sum_{\mu=1}^{n} \lambda_{\mu i}}{\sum_{\mu=1}^{N_i} |\lambda_{\mu i}|} \tag{4}$$

where N_i is the number of components within the ith subject, λ_μ is the μth largest eigenvalue, $\frac{1}{k_i}$ is the fraction of total components considered to be neighbors and n is the number of eigenvalues used to describe the subject's distance matrix such that $n \leq 10 \leq N_i$. The upper bound of 10 is selected as a search parameter range since all $N_i \geq 10$. The BIC for a subject's embedding of N_i components using k_i is

$$\text{BIC}(N_i, k_i, n) = -2*\log\left(L_{(k_i, n)}\right) + k_i*\log(N_i) \tag{5}$$

For a given n, select the k_i that minimizes the BIC for that subject. The k_i is treated as the degrees-of-freedom parameter because a neighborhood size is calculated as $\frac{N_i}{k_i}$. If k_i increases, the neighborhood size decreases, and there are fewer connections defined between nodes on the graph. This leads to an increased flexibility in the location which points can take. More connections necessarily lead to more restrictions on how the object can be embedded. Because of this, the BIC of the model bears an inverse relationship to the connectedness of the graph. As k_i increases, the connectivity decreases and the BIC increases.

The eigenvalue dimension, or eigendimension, indicates the number of eigenvalues used in the classifier. The eigendimension parameter n must be held constant across all subjects in order to train a classifier, so a random forests model is created for all $n \in (1,10)$, where the parameter k_i will be selected to maximize the goodness of fit as described above. The eigendimension parameter n is selected that maximizes the classification accuracy across subjects.

The results are presented in Table 1.

Although the accuracy is decreasing with sample size, the relative classification accuracy with respect to chance *improves* with sample size. When trying to increase the number of possible labels in a set, the chance rate of accuracy decreases. With multivariate classification, the "chance" accuracy classification rate (Alzheimer's/old/young) was 34.1%, whereas with the bivariate classification of subgroups (Alzheimer's, old), (Alzheimer's, young), and (old, young) the "chance" accuracy rate was 51.9%, 51.9%, and 50%, respectively. Relative to the chance accuracy, the multivariate classifier actually has improved results with more samples, with respective accuracy ratios of classification accuracy/chance accuracy of 1.9326 for the multivariate classification compared to 1.6416, 1.4277, 1.7206 classification ratios for the bivariate runs, using Method 2 accuracy results in Table 2.

An investigation into the classification error within category are discussed in Misclassification error rates.

Method 2: Optimized dual parameter selection

In this section we present a method where the two parameters n and k for fitting the neighborhood are optimized simultaneously within the model. Both n and k are global parameters and are constant across subjects. The out-of-bag error using this approach is artificially lower than the testing error. Because two parameters are being optimized with respect to the out-of-bag error, *Method 2* produces a more biased estimate of the training error than does *Method 1*, which optimizes only a single parameter. This hypothesis is tested below, when cross-validation is run outside of the random-forests parameter selection stage.

The neighborhood size parameter k will be held constant across all subjects within each model evaluation, where $k \in (2,10)$. The eigenvalue dimension $n \in (1,10)$.

The results appear in Table 2.

Because there may exist multiple pairs (n^*, k^*) corresponding to the same maximum classification accuracy over all possible parameter combinations (n, k), we select the minimum n yielding the optimal accuracy. In the event that multiple (n, k) pairs yield the same classification accuracy for the smallest n, the minimal k is use as a tiebreaker. For example, in the schizophrenia/normal dataset, there were 9 total (n^*, k^*) combinations yielding 90% classification accuracy, so the smallest n rule yielded a (n^*, k^*) parameter pair as $(2, 10)$.

Cross-validation

Both *Method 1* and *Method 2* optimized neighborhood fit parameters by minimizing the out-of-bag error, or maximizing the out-of-bag-accuracy. To compensate for the bias created by training our classifier on the out-of-bag error, we performed leave-one-out cross-validation on top of the resampling already involved in the random forests procedure. This cross-validation is performed *outside* of the entire model fitting and parameter selection stage to ensure that the testing-accuracy remains unbiased (Simon et al., 2003; Demirci et al., 2008). A single observation is omitted from the dataset containing n observations, the model is constructed using the $n - 1$ observations with the eigendimension parameter and neighborhood

Table 1
Selection of single embedding parameter.

Classification accuracy				
Groups	Maximum accuracy	Eigenvalue dimension	Median accuracy	Chance accuracy
Alzheimer's, old, young	65.9%	1	50.0%	34.1%
Alzheimer's, old	74.1%	1	48.2%	51.9 %
Alzheimer's, young	74.1%	1	66.3%	51.9 %
Old, young	89.3%	1	66.1%	50 %
Schizophrenic, normal	80%	3	80%	70%

Table 2
Selection of dual embedding parameters.

Classification accuracy					
Groups	Maximum accuracy	Eigenvalue dimension	Nearest neighbors	Median accuracy	Chance accuracy
Alzheimer's, old, young	65.9%	1	1/2	51.2%	34.1%
Alzheimer's, old	85.2%	1	1/4	63.0%	51.9%
Alzheimer's, young	74.1%	2	1/7	70.4%	51.9%
Old, young	89.3%	1	1/2	71.4%	50%
Schizophrenic, normal	90%	3	1/10	80%	70%

Table 3
Accuracy over methods.

Cross-validation accuracy			
Groups	Method 1 CV accuracy	Method 2 CV accuracy	Chance accuracy
Alzheimer's, old, young	65.9%	53.7%	34.1%
Alzheimer's, old	74.1%	74.1%	51.9%
Alzheimer's, young	62.9%	59.3%	51.9%
Old, young	89.2%	89.2%	50%
Schizophrenic, normal	80%	80%	70%

size parameter optimized as above. The predictive model is chosen with the eigendimension that maximizes the classification accuracy (minimizes the out-of-bag error) on the $n - 1$ observations, and this model is then tested on the nth observation that was originally set aside. This procedure is performed repeatedly leaving out a single observation each time for the entire dataset, and the classification accuracy is computed based on the cross-validation accuracy leading to a truly unbiased estimate. The results are shown in Table 3.

A difference between the cross-validation and out-of-bag error cannot be interpreted directly as a measure of bias in the original model creation. Because of the relatively small sample size, leaving out a single observation significantly reduces the dataset size on which the model is created. For example, using *leave-one-out* on the schizophrenia/normal dataset reduces the training set size by 5%. A difference between the out-of-bag error and the cross-validation error then may be attributed to this difference, and not because of bias introduced with the parameter optimization procedure.

Because there may exist multiple (n^*, k^*) parameters that yield the same maximal classification accuracy in *Method 2*, there exists some flexibility in the choice of (n, k) on which to estimate the cross-validation accuracy. For simplicity, here we use the (n, k) pair with the smallest n over all pairs yielding the same maximal classification accuracy. If there exists more than one (n, k) corresponding to the maximal classification accuracy and the same minimum n, we then select the pair with the minimum k as well. This is equivalent to the n, k chosen to represent the eigenvalue dimensions in *Method 2*. For further details see Sensitivity to parameter choice.

Sensitivity to distance metric choice

In this section we will test the methods developed above using three other distance metrics: the correlation distance, the fractal distance, and a new metric we call the phase distance. In this manner we will see how sensitive spectral classification is to the distance metric used to describe the association between independent components.

Correlation

The cross-correlation of two timeseries is merely a lagged version of the correlation. The correlation is a linear metric describing the relationship between increases and decreases in signal amplitude over time.

$$\text{Correlation}\left(M_\alpha, M_\beta\right) = \frac{E\left[\left(m_{\alpha,t} - \overline{M_\alpha}\right)\left(m_{\beta,t} - \overline{M_\beta}\right)\right]}{\sqrt{E\left[\left(m_{\alpha,t} - \overline{M_\alpha}\right)^2\right]E\left[\left(m_{\beta,t} - \overline{M_\beta}\right)^2\right]}} \quad (6)$$

Results using this metric are shown in Table 4.

Phase distance

To quantify the relationship between pairs of components within a subject, we will create a metric called phase distance that measures the change in activation levels between pairs of components over time.

A shift in energy between two timecourses M_α and M_β between time $(t, t+1)$ can be calculated as the Euclidean distance

$$D_{\text{E}}\left(m_{\alpha,t}, m_{\beta,t}\right) = \sqrt{\left(m_{\alpha,t} - m_{\alpha,t-1}\right)^2 + \left(m_{\beta,t} - m_{\beta,t-1}\right)^2} \quad (7)$$

This is an extension of the univariate concept of "phase distance", where univariate movement over time is plotted with the two axis being the observation at time $(t, t+1)$. Performing this calculation over the range of time yields a vector, $D_{\text{E}}(M_\alpha, M_\beta)$.

Table 4
Correlation metric.

Classification accuracy				
Groups	Method 1 RF accuracy	Method 1 CV accuracy	Method 2 RF accuracy	Method 2 CV accuracy
Alzheimer's, old, young	61.0%	42.9 %	65.9%	58.5%
Alzheimer's, old	63.0%	59.3%	70.4%	37.0 %
Alzheimer's, young	81.5%	74.1%	81.4%	63.0%
Old, young	82.1%	71.4 %	92.9%	71.4 %
Schizophrenic, normal	80%	75%	90%	70%

If this energy shift were systematic, one could argue there existed a relationship between the independent components represented by M_α and M_β. The periodogram of the distance vector $D_{\text{E}}(M_\alpha, M_\beta)$ would exhibit dominant frequencies if this energy shift were ordered, and equal amplitude at all frequencies if there was no regular pattern. "White noise" is defined by this equal distribution of amplitude across all frequencies, and the variance of the amplitudes across all frequencies would be small. A dominant frequency would increase the standard deviation of the periodogram frequencies.

The phase distance between two independent components timecourses is constructed around the regularity of energy shifts among pairs of independent component timecourses.

$$d\left(M_\alpha, M_\beta\right) = \frac{1}{SD\left(D_E\left(M_\alpha, M_\beta\right)\right)} \quad (8)$$

This metric is calculated for all possible component pairs within a subject to form a distance matrix. Results using this metric are shown in Table 5.

Fractal correlation dimension

A fractal measure of dimensionality is used to quantify the complexity of this bivariate trajectory. The correlation dimension (Grassberger and Procaccia, 1983) computes the dimensionality of a space occupied by a set of random points, and is measured as a density limit of the number of points contained within an ε-ball where the number of points sampled approaches infinity as the radius of the ball ε approaches zero. We compute the density of points in a two-dimensional space, where the first dimension is the set of points M_α, and the second dimension is the set M_β. A single point in the space at time t is $(m_\alpha, m_{\beta,t})$. Although these points are embedded in a two-dimensional space, the distribution of the fractal dimension of these points is bounded above by two and is actually lower than this.

The fractal dimension is calculated using a parameter called the confidence parameter, α, which allows extremely distant points in the set to be removed. This reduces the effects of possible outliers in the calculation by removing an observation that is atypical with respect to the other points. The default parameter in R of $\alpha = .2$ is used here.

Results using this metric are shown in Table 6.

The results for this metric are suboptimal with respect to the other parameters. A reason for this may be in the instability of this metric because of the number of points. The fractal dimension is an estimate

Table 5
White-noise metric.

Classification accuracy				
Groups	Method 1 RF accuracy	Method 1 CV accuracy	Method 2 RF accuracy	Method 2 CV accuracy
Alzheimer's, old, young	48.8%	29.3 %	58.5%	46.3%
Alzheimer's, old	70.4%	59.3%	85.2%	81.4%
Alzheimer's, young	51.9%	29.6%	81.4%	70.4%
Old, young	64.3%	57.2 %	78.6%	75%
Schizophrenic, normal	80%	75%	75%	75%

t7.1 **Table 6**
t7.2 Fractal dimension metric.

Classification accuracy				
Groups	Method 1 RF accuracy	Method 1 CV accuracy	Method 2 RF accuracy	Method 2 CV accuracy
Alzheimer's, old, young	53.7%	41.5 %	53.7%	36.7%
Alzheimer's, old	55.6%	37.0%	63.0%	22.2%
Alzheimer's, young	77.8%	63.0%	77.8%	55.6%
Old, young	67.9%	60.7 %	78.6%	39.3 %
Schizophrenic, normal	80%	75%	85%	75%

625 of density as $N \rightarrow \infty$, however our N here is limited to roughly 125
626 points for both datasets. As such, the number of points we have may
627 lead to instable estimates of an infinite limiting density.

Sensitivity to parameter choice

629 Here we will examine the effect the parameter choice has on the
630 classification accuracy.

Method 1: Single parameter optimization

632 Method 1 discussed the selecting model parameters (n, k_i) such
633 that k_i is selected within a subject by optimizing a model fit, and n is
634 optimized with respect to minimizing the classification error over all
635 subjects. We will discuss here the change in classification accuracy
636 associated with the change in n.
637 For the schizophrenia/normal dataset, the maximal classification
638 accuracy was obtained with eigenvalue dimension $n = 3$, and the
639 accuracy stayed constant with successive dimensions in Fig. 5. This is
640 an indicator that the smaller dimensions were the better predictors at
641 between-group differences. For the Alzheimer's/old/young dataset,
642 the maximal classification accuracy was obtained with an eigendi-
643 mension of $n = 1$ in Fig. 6. Extracting successive eigenvalues into the
644 feature vector served to lower the classification accuracy.

Method 2: Dual parameter optimization

646 The procedure has two free parameters that are optimized: the
647 eigendimension n and the neighborhood size k.
648 The number of principal eigenvalues used to create a feature
649 vector for a subject is a free parameter bounded above by the
650 minimum number of components existing over all subjects. The
651 number of eigenvalues n used to construct a classifier are by
652 themselves an indicator of the level of variation among the groups;
653 if there existed significant differences between groups, one would see
654 a large number of principal eigenvalues along which there existed
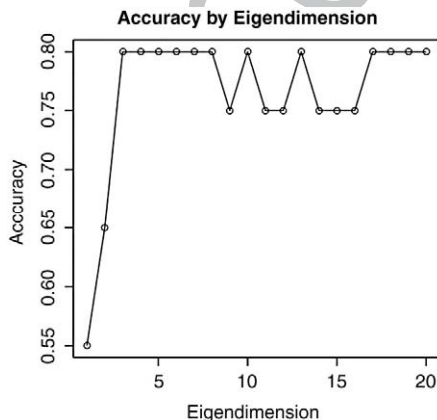655 between-group variations.

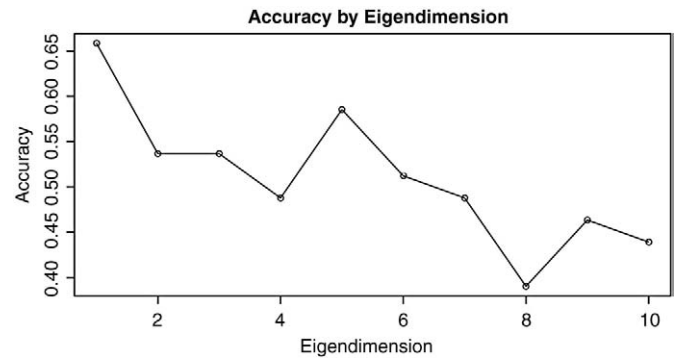**Fig. 5.** SZ accuracy by extracted eigenvalues.

Fig. 6. AD accuracy by extracted eigenvalues.

656 Another parameter to be selected is the fraction of nearest-
657 neighbors to be considered when calculating the geodesic distances.
658 Because all subjects had a unique number of components, we will take
659 a constant percentage of the total number of components to
660 determine the neighborhood size. The eigenvalue dimension will be
661 selected between 1 and 10, while between 10% and 50% ($\frac{1}{k}, k \in (2, 10)$)
662 of the total number of components within a subject will be used for
663 neighborhood selection.
664 We will examine the influence of these parameters on the
665 classification accuracy by altering the free parameters.
666 As shown in Fig. 7, the accuracy of the classifier for the Old/Young/
667 Alzheimer's dataset improves when using smaller numbers of
668 eigenvalues, which is an indicator that the most difference exists
669 among the first few dimensions. The trend is not as clear in the effect
670 of neighborhood size in the predictive accuracy. The dashed line
671 indicates the random classification accuracy of 33.3%. The median
672 classification accuracy was 51.4%, and the maximum accuracy was
673 65.9%. The distribution of the accuracy for all possible free parameters
674 for the Alzheimer's/old/young dataset shows a unimodal shape with
675 the middle 50% of parameters having accuracy between 46.4% and
676 53.7%.
677 For the schizophrenia/normal dataset the accuracy of the classifier
678 improves using greater numbers of eigenvalues in Fig. 8. This may be
679 true because there existed initially more components in this dataset
680 than the Alzheimer's/old/young dataset, which would lead to a
681 greater number of dimensions on which to discriminate. Similar to the
682 first dataset, there does not appear to be a consistent pattern between
683 the neighborhood size and classification accuracy. The distribution of
684 accuracies over all possible parameters is roughly symmetric with a
685 left skew.

Conclusion

687 The methods developed here can be seen as comparing interac-
688 tions of spatially independent components over time within a subject
689 and seeking differences in these interactions across groups. Mathe-
690 matically, we are trying to discriminate among distance matrices,
691 while geometrically we are comparing a group of points (compo-
692 nents) in some unknown subject-defined space to another group of
693 points in a different subject's space. Using the geodesic similarity
694 unwinds the shape that each group of point forms, thereby increasing
695 the effectiveness of a linear eigendecomposition on a non-linear
696 subspace. Then, we extract the eigenvalues of the similarity matrix to
697 obtain the strength of the primary dimensions. We are then
698 comparing the size of our unknown manifolds along the primary
699 dimensions across subjects and using differences across subjects to
700 construct a classifier.
701 We have demonstrated that the temporal information alone
702 contains a signal strong enough for discrimination. The eigenvalue
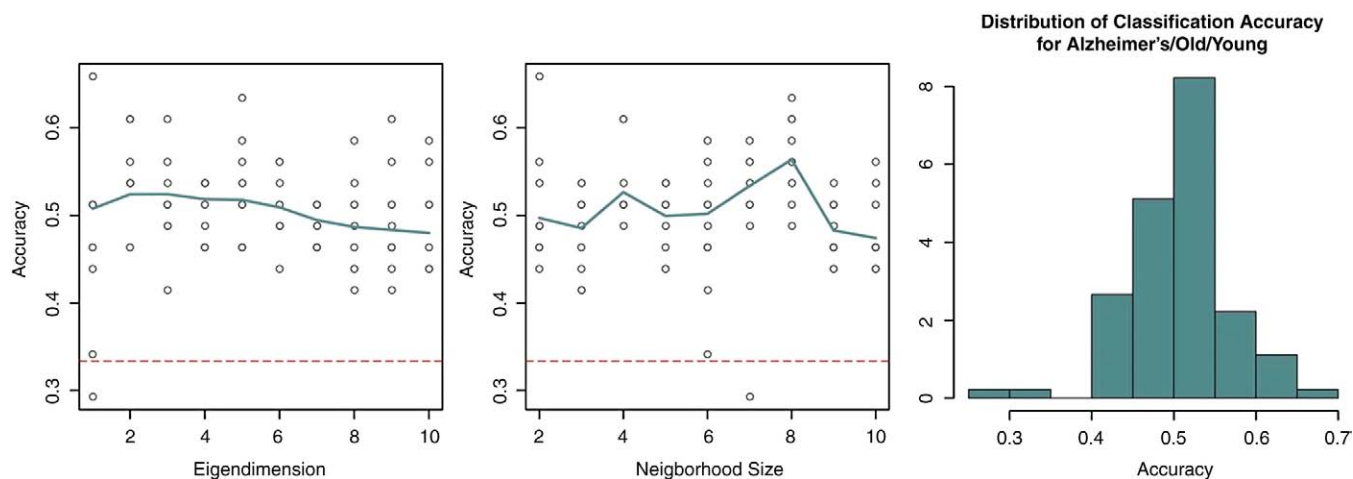703 dimension indicates the number of principal eigenvalues along which

Fig. 7. AD parameter choice.

the groups exhibit significant variation. The need for the geodesic distance transformation demonstrated that the temporal connectivity among the components is highly non-linear. This may be related to the non-linearity of the initial dimension reduction method ICA. The geodesic transformations of the association matrices smooth the non-linear manifold joining components, improving the features extracted during the eigen-decomposition.

A proposed future direction is to combine spatial and temporal classification models to create a more powerful time–space hybrid classifier. Both methods offer valuable discriminative power along different domains, so a combination could only serve to strengthen existing models. In addition, the existing algorithm could developed using aligned scans with group component extraction, which would allow one to identify what hypothesized neurological networks behave differently across groups. This would allow direct comparisons of components across subjects instead of comparing properties of subject connectivity.

The approach presented here circumvents many problems that otherwise make classification based on neuroimaging data difficult. First we perform dimension reduction using a method, ICA, that extracts discriminating features of the images automatically. ICA can be seen as an element from a class of dimension–reduction methods that effectively extract basis functions that describe the images in a compact manner. Although there were 125 total possible independent components within a randomly selected normal subject, the top

10 independent components sorted by variance explained cumulatively were able to explain roughly 27.0% of the total temporal variance. The independent components have the further attractive feature that the spatial signatures are reported by neuroscientists in many cases to correspond roughly to identifiable functional networks. Thus our classifier may be operating on meaningful functional architecture of the brain. Our method operates using all the independent components within a subject, so no human interpretation is required to achieve classification of the data. Because of the anatomical variability of human brains – and presumably the added variability of the presence of certain function circuits – as crucial advantage of our method is the obviation of the need for structural alignments.

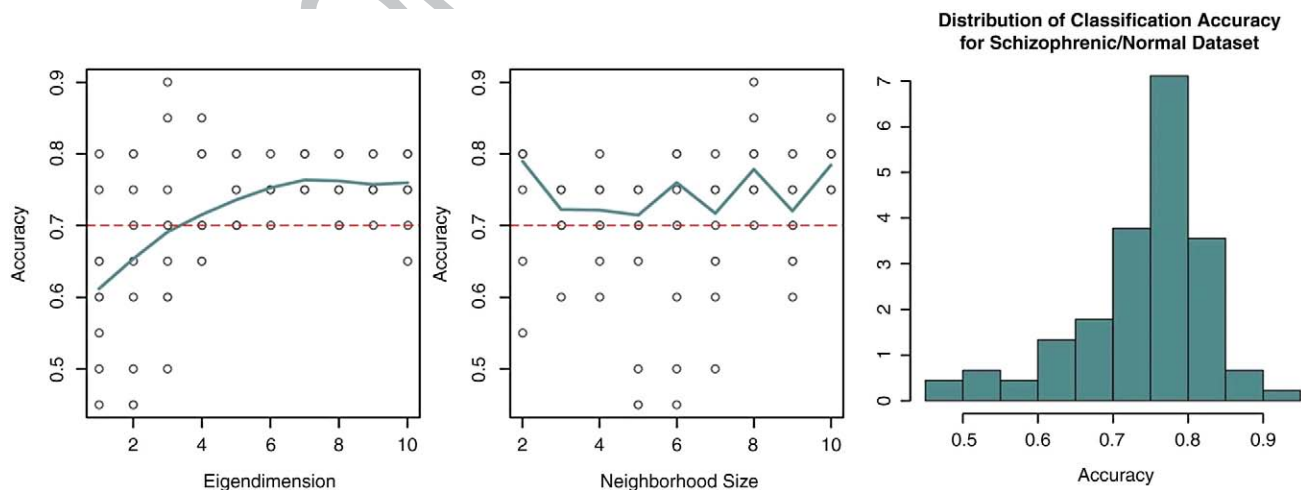**Fig. 8.** SZ parameter choice.
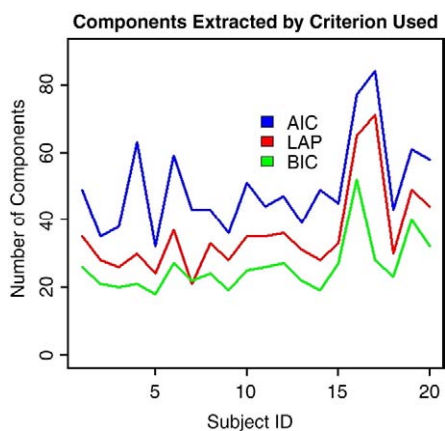
Components Extracted by Criterion Used

Fig. 9. Number of components extracted by selection method.

Appendix

As the procedure was created with the free parameters of neighborhood size choice and eigendimension, we wish to see how the selection of these parameters changes the accuracy of the classifier. We also will discuss how the algorithm methods presented here relates to two popular machine-learning algorithms: ISOMAP (Tenenbaum et al., 2000) and spectral clustering (Ng et al., 2001).

Sensitivity to component number approximation method

The number of components was initially chosen using the laplace approximation to the model order (LAP) (Minka, 2000), which has been found previously to best estimate the number of ICAs in a subject compared to other methods such as Akaike information criterion (AIC), Bayesian information criterion (BIC), and the minimum description length (MDL). We will examine the impact of changing the method in which the number of independent components are selected within the schizophrenia/normal dataset by comparing the results using LAP to select the parameters compared to AIC and BIC.

There exists a consistent trend in the number of components extracted by criterion method used, shown in Fig. 9. The AIC consistently estimates the greatest number of components, while the LAP is second, and the BIC selects the lowest number of components. Using the components extracting for each of these three methods, we will investigate the effect changing the criterion has on classification accuracy using Method 1 and Method 2 for the schizophrenia/normal Dataset.

Changing the estimation method yields lower classification methods for both criteria using Method 1, yet yields slightly better results for BIC than LAP in Method 2, as shown in Table 7. As Method 2 is a biased estimate of the testing error because of its extreme use of parameter optimization, this result may be a result of overfitting. As the LAP method has previously been shown to be the best manner of estimating the number of component sources, it appropriately yields the highest average accuracy over the other selection methods of AIC and BIC.

Table 7
SZ/normal method dependency.

Classification accuracy by component selection criterion				
Criterion	Method 1 accuracy	Eigenvalue dimension	Method 2 accuracy	Eigenvalue dimension
AIC	65%	5	75%	1
BIC	70%	7	95%	8
LAP	80%	3	90%	3

Table 8
Method 1 AD/young/old errors.

Misclassification matrix				
Variable	Young	Old	Alzheimer's	Classification error
Young	9	2	3	35.7%
Old	1	11	2	21.4%
Alzheimer's	2	4	7	46.2%

Misclassification error rates

The misclassification rate by category is shown for both datasets using the optimal model selected in Method 1.

For the Alzheimer's/old/young dataset, the easiest category to identify was *old*, while the most difficult category to identify was *Alzheimer's* in Table 8.

The missclassification matrix for the bivariate schizophrenia/normal classification run shows that the easiest class to identify was the *normal* category, while the most difficult was the *schizophrenia* class in Table 9.

Relationship to existing methods

Independent components analysis (ICA)

The methods presented here are largely dependent upon the initial step of dimension reduction, where ICA is used to decompose the data into source signals.

ICA operates under the assumption that an observation x is actually a linear combination of independent source signals s_i such that $x = As$ (Hyvärinen and Oja, 2000). The source signals are assumed to be non-Gaussian, because if they were Gaussian and independent the estimating multivariate Gaussian joint distribution would be symmetric, thus leading to source estimations that are estimable only up to orthogonal rotations. The algorithm used for this analysis, FAST-ICA, estimates the source signals by maximizing the negentropy using Newton's method.

ISOMAP

This classification method uses concepts from the ISOMAP algorithm (Tenenbaum et al., 2000) which transforms a Euclidean distance matrix into a geodesic distance matrix before projecting the data on the principal eigenvectors corresponding to the principal eigenvalues. ISOMAP can be understood as a geodesic transformation of a distance matrix followed by traditional multidimensional scaling. While spectral classification transforms the distance matrix using geodesic distances, spectral classification uses the eigenvalues of the primary dimensions for classification rather than using the principal eigenvectors for projection. Calculating the geodesic distances transforms the original distance matrix into a weighted adjacency matrix by using nearest neighbors to determine adjacency.

Spectral clustering

Spectral clustering procedures group points using on the spectral properties of the Laplacian matrix of a graph (Ng et al., 2001). For a weighted adjacency matrix $W_{(n,n)}$ that gives the weighted connections for n points, the degree of a point is defined as $d_i = \sum_{j=1}^{n} w_{ij}$. If two points i and j are not connected, $w_{ij} = 0$. For a set of n points the degree matrix $D_{(n,n)}$ is a diagonal matrix where $a_{ij} = \text{degree}(i)$ if $i = j$, and 0 otherwise. The adjacency matrix $A_{(n,n)}$ describes the connectivity of a

Table 9
Method 1 SZ/normal errors.

Misclassification matrix			
Variable	Schizophrenic	Normal	Classification error
Schizophrenic	4	2	33.3%
Normal	2	12	16.7%

graphs, where $a_{i,j} = 1$ if points i and j are connected, and 0 otherwise. The Laplacian of a graph then is computed as $L = D$ - A. Spectral clustering operates by extracting the eigenvectors of L that correspond to the minimum eigenvalues and creating a matrix V with the columns of V corresponding to the eigenvectors of L. Points y_i are constructed by taking the rows of V and are clustered into a predetermined number of k groups using the k-means clustering technique.

Spectral classification differs from spectral clustering by using a spectral decomposition of the weighted adjacency matrix W instead of the Laplacian L of W. The principal eigenvalues are used for classification in spectral classification, while the minimal eigenvectors are used for clustering in spectral clustering.

References

Breiman, L., 2001. Random forests. Mach. Learn. 45, 5–32.

Buckner, R.L., Snyder, A.Z., Sanders, A.L., Raichle, M.E., Morris, J.C., 2000. Functional brain imaging of young, nondemented, and demented older adults. J. Cogn. Neurosci. 12 (Supplement 2), 24–34.

Calhoun, V.D., Maciejewski, P.K., Pearlson, G.D., Kiehl, K.A., 2007. Temporal lobe and default hemodynamic brain modes discriminate between schizophrenia and bipolar disorder. Hum. Brain Mapp. 9999 (9999) NA+.

Demirci, O., Clark, V., Magnotta, V., Andreasen, N., Lauriello, J., Kiehl, K., Pearlson, G., Calhoun, V., 2008. A review of challenges in the use of fMRI for disease classification/characterization and a projection pursuit application from multi-site fMRI schizophrenia study. Brain Imag. Behav. 2 (3).

Ford, J., Farid, H., Makedon, F., Flashman, L.A., Mcallister, W., Megalooikonomou, V., Saykin, A.J., 2003. Patient classification of fMRI activation maps. Proc. of the 6th Annual International Conference on Medical Image Computing and Computer Assisted Intervention (MICCAI'03, 58–65.

Grassberger, P., Procaccia, I., 1983. Measuring the strangeness of strange attractors. Phys. D: Nonlinear Phenom. 9 (1-2), 189–208.

Hogg, R.V., Craig, A., Mckean, J.W., June 2000. Introduction to Mathematical Statistics (6th Edition).

Hyvärinen, A., Oja, E., 2000. Independent component analysis: algorithms and applications. Neural. Netw. 13 (4-5), 411–430.

Jafri, M.J.J., Pearlson, G.D.D., Stevens, M., Calhoun, V.D.D., November 2007. A method for functional network connectivity among spatially independent resting-state components in schizophrenia. NeuroImage.

Damoiseaux, J.S., Rombouts, S.A., F.B.P.S.C.S.S.S.C.B., 2006. Consistent resting-state networks across healthy subjects. Proc. Natl. Acad. Sci.

Kruskal, J., March 1964. Multidimensional scaling by optimizing goodness of fit to a nonmetric hypothesis. Psychometrika 29 (1), 1–27.

Minka, T.P., 2000. Automatic choice of dimensionality for PCA. Tech. rep., NIPS.

Ng, A.Y., Jordan, M.I., Weiss, Y., 2001. On spectral clustering: Analysis and an algorithm. MIT Press.

R Development Core Team, 2008. R: A Language and Environment for Statistical Computing. R Foundation for Statistical Computing, Vienna, Austria, ISBN 3-900051-07-0. URL http://www.R-project.org.

Ridha, B.H., Barnes, J., Bartlett, J.W., Godbolt, A., Pepple, T., Rossor, M.N., Fox, N.C., 2006. Tracking atrophy progression in familial Alzheimer's disease: a serial MRI study. Lancet Neurol. (10), 828–834 October.

Roebroeck, A., Formisano, E., Goebel, R., 2005. Mapping directed influence over the brain using granger causality and fmri. NeuroImage 25 (1), 230–242 March http://dx.doi.org/10.1016/j.neuroimage.2004.11.017.

Shenton, M., Dickey, C., Frumin, M., McCarley, R., 2001. A review of MRI findings in Schizophrenia. Schizophr. Res. 49, 1–52.

Simon, R., Radmacher, M.D., Dobbin, K., McShane, L.M., 2003. Pitfalls in the use of DNA microarray data for diagnostic and prognostic classification. J. Natl. Cancer Inst. 95 (1), 14–18 http://jnci.oxfordjournals.org.

Smith, S.M., Jenkinson, M., Woolrich, M.W., Beckmann, C.F., Behrens, T.E.J., Johansen-berg, H., Bannister, P.R., Luca, M.D., Drobnjak, I., Flitney, D.E., Niazy, R.K., Saunders, J., Vickers, J., Zhang, Y., Stefano, N.D., Brady, J.M., Matthews, P.M., 2004. Advances in functional and structural MR image analysis and implementation as FSL. NeuroImage 23, 208–219.

Tenenbaum, J.B., de Silva, V., Langford, J.C., 2000. A global geometric framework for nonlinear dimensionality reduction. Science 290 (5500), 2313–2319.

Woods, R.P., Grafton, S.T., Watson, J.D., Sicotte, N.L., Mazziotta, J.C., 1998. Automated image registration: II. Intersubject validation of linear and nonlinear models. J. Comput. Assist. Tomogr. 153–165.

Zhang, L, Samaras, D., 2005. Machine learning for clinical diagnosis from functional magnetic resonance imaging. IEEE Conference on Computer Vision and Pattern Recognition (CVPR, 1211–1217.